Preprint
UCRL-JC-144912

Internal Stress Plasticity-Creep Due to Dynamic Hydrogen Gradients in Ti-6A14V

C. Schuh, D. C. Dunand

This article was submitted to
131st Annual Meeting and Exhibition of the Minerals, Metals and Materials Society, Seattle, WA, February 17-21, 2002

U.S. Department of Energy

Lawrence
Livermore
National
Laboratory

September 10, 2001

This work was performed under the auspices of the United States Department of Energy by the University of California, Lawrence Livermore National Laboratory under contract No. W-7405-Eng-48.

INTERNAL STRESS PLASTICITY-CREEP DUE TO DYNAMIC HYDROGEN GRADIENTS IN Ti-6Al-4V

C. Schuh[1,2] and D. C. Dunand[1]
[1] Department of Materials Science and Engineering, Northwestern University, Evanston, IL
[2] Materials Science and Technology Division, Lawrence Livermore National Laboratory, Livermore CA

Abstract

Internal-stress plasticity is a Newtonian creep mechanism which operates at low applied stress levels, when there is a concurrent internal stress. Common sources of internal stress are thermal-expansion or phase-transformation mismatch; in this work we explore the possibility of chemically-induced internal stresses. We report tensile creep experiments on the BCC β-phase of Ti-6Al-4V, in which dynamic gradients of hydrogen concentration were introduced through cycling of the test atmosphere (between Ar/H_2 mixture and pure Ar) under low applied stresses. Under these conditions, we observe Newtonian deformation at rates much higher than for constant-composition conditions, as expected for internal stress plasticity. Also, we present an analytical model which considers chemical, elastic, and creep strains during chemical cycling under stress, and find good agreement with the experimental results.

Introduction

The phenomenon of internal stress plasticity is observed in materials which are externally stressed while simultaneously experiencing internal mismatch strains [1]. The external stress biases these mismatch strains, which develop (by a plastic deformation mechanism such as power-law creep) preferentially in the direction of the external stress. Internal stress plasticity is characterized by two main features at low applied stresses. First, the global deformation obeys a linear flow law, where the average strain rate during cycling is proportional to the applied stress. Second, because of its low stress exponent, internal stress plasticity occurs at a faster rate than creep in the absence of internal stresses. The combination of high flow stability and rapid deformation at low stresses makes internal stress plasticity of interest in shape forming; after multiple thermal or pressure cycles, this mechanism often leads to very large tensile elongation (> 100%) and is thus described as *internal stress superplasticity* [1].

Internal stress plasticity is commonly observed during thermal cycling, where internal mismatch strains develop due to (i) thermal expansion mismatch between coexisting phases, as in metal matrix composites [2-5], (ii) thermal expansion mismatch between adjacent grains in an anisotropic solid [6-8], or (iii) density mismatch between polymorphic phases during a solid/solid phase transformation [9-16]. Recently, some investigators have demonstrated internal stress plasticity during pressure cycling, at constant temperature, due to (i) compressibility mismatch between phases in a composite (in Al/SiC, in uniaxial tension or during powder compaction [17, 18]), and (ii) pressure-induced allotropic phase transformation (in H_2O ice [19]).

In addition to thermal and pressure cycling, there is a possibility of inducing internal stress plasticity by cycling the chemical composition of a material while subjecting it to an external stress. For example, during a cyclic process of charging and discharging of a material with a gaseous species, the absorption of diffusant leads to a swelling expansion of the crystal lattice. Because of concentration gradients of the diffusing species, a swelling gradient is established, leading to so-called chemical stresses [20]. At low temperatures, these stresses are accommodated elastically while at elevated temperatures, they may be accommodated by creep, thus opening the possibility of inducing internal stress plasticity if an external stress is applied.

In the present work, we measure the tensile deformation of the engineering alloy Ti-6Al-4V at 1030° C (in the β phase) under conditions of cyclic charging/discharging with hydrogen, which dissolves interstitially in the alloy. We demonstrate that chemical strain gradients are sufficient to induce internal stress plasticity. Additionally, we present an analytical model that considers the superposition of internal chemical stress with an external uniaxial stress, and compare the model predictions to the present experiments.

Experimental Procedures

Powder metallurgy Ti-6Al-4V billets (from Dynamet Technology, Burlington, MA) were machined into tensile specimens of 20-mm gauge length and 5-mm gauge diameter. Tensile deformation experiments were conducted in a custom creep apparatus described in Ref. [15], at a constant temperature of 1030° C, monitored by a type-K thermocouple in contact with the specimen gauge. Deformation of the specimen was measured with a linear voltage-displacement transducer at the cold end of the load train. Two different test atmospheres were used during the experiments; high-purity argon (99.999%) and a mixture of high-purity argon with 3.66% H_2. At atmospheric pressure, these two atmospheres correspond to hydrogen partial pressures of $P_{H2} = 0.0$ and 3.8 kPa, respectively. The gas flow rate was maintained at 1.3 l/min, so that the volume of gas in the test apparatus was exchanged about every 25 seconds. Gas was

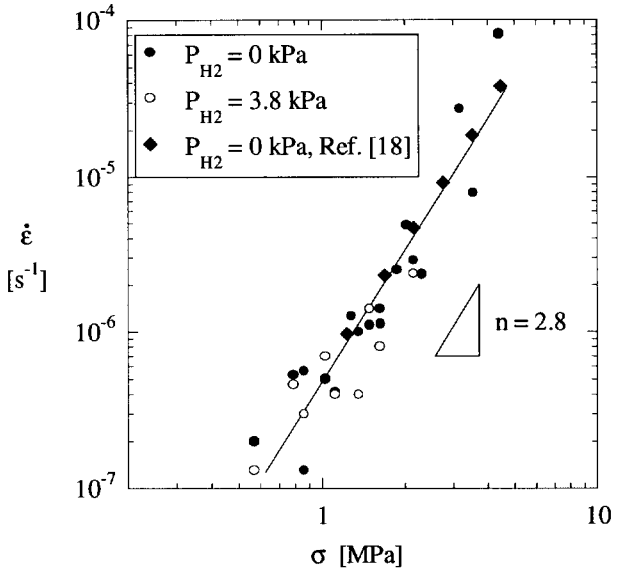

Figure 1: Isothermal creep rate of Ti-6Al-4V as a function of the uniaxial tensile stress at 1030° C, in a high-purity argon atmosphere as well as the Ar/H_2 mixture.

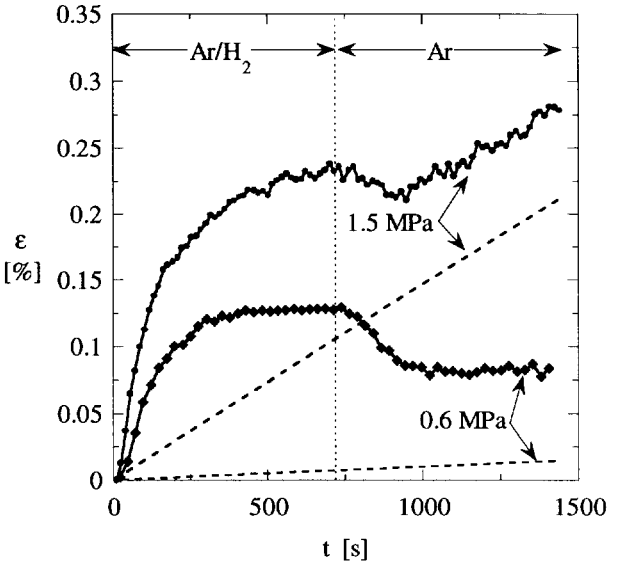

Figure 2: True strain history of Ti-6Al-4V during 24-minute chemical cycles at 1030° C, compared to the expected creep history for a specimen with constant composition deforming in pure Ar or Ar/H_2 mixture (dashed lines).

introduced into the apparatus through a sprayer to ensure that the flow of gas was turbulent around the specimen, preventing concentration gradients in the test atmosphere.

Tensile deformation was investigated at 1030° C during cycling of the test atmosphere between P_{H2} = 0.0 and 3.8 kPa. Two types of cycles were used, with periods of 24 and 30 minutes. Thus, during a single cycle, specimens were exposed to 12 or 15 minutes of the Ar/H_2 mixture, followed by an equal exposure to the high-purity Ar atmosphere. In every case, at least 3 consecutive chemical cycles were performed to insure a dynamic steady-state, and to verify reproducibility of the specimen length changes during chemical cycling. Isothermal creep data was also collected at 1030° C at various small stresses (0.5-5 MPa) in both static test atmospheres (Ar and Ar/H_2).

Results and Discussion

At the test temperature of 1030° C, Ti-6Al-4V is single phase, with Al and V in solid solution within BCC β-Ti [21]. Furthermore, the dissolution of hydrogen in the β-Ti phase of Ti-6Al-4V causes no phase transformation [22]. Thus, for all of the experimental conditions examined in this work, the material was in the β-phase field. The microstructure both before and after the high-temperature experiments was found to consist of large (100-400 μm) prior-β grains.

The isothermal creep data at 1030° C are shown in Fig. 1, with the uniaxial strain rate $\dot{\varepsilon}$ plotted against the applied tensile stress σ. The strain rate data exhibits a power-law stress dependence:

$$\dot{\varepsilon} = K \cdot \sigma^n \qquad (1)$$

with a stress exponent n close to three and with some scatter between different specimens. The test atmosphere (Ar or Ar/H_2) did not appreciably affect the creep behavior of the alloy, as also reported for unalloyed Ti for these low strain rates and hydrogen pressures [23]. All of the data can be fitted to Eq. (1) with values of $K = 4.8 \cdot 10^{-7}$ $MPa^{-2.8}$ and n = 2.8. These parameters are

very close to those obtained in our recent work [13] on hydrogen-free Ti-6Al-4V at the same temperature ($K = 4.7 \cdot 10^{-7}$ $MPa^{-2.8}$ and $n = 2.8$), and are in broad agreement with earlier results for deformation of hydrogen-free Ti-6Al-4V at similar temperatures (1000-1100° C) but higher stresses (6.4-160 MPa) [24, 25].

During chemical cycling, the average deformation rates were larger than for creep under isochoral (i.e., constant-composition) conditions in either Ar or Ar/H_2. Typical results are shown in Fig. 2 for the 24-minute cycles, where the true strain of the specimen gauge is plotted as a function of time during the chemical cycles. Similar curves were obtained for the 30-minute cycles. During exposure to gaseous H_2, the specimen interstitially absorbs atomic hydrogen and the crystal lattice swells, giving rise to a transient increase in specimen length. On the second half of the cycle, during annealing in pure Ar, the dissolved hydrogen diffuses to the specimen surface and escapes into the hydrogen-free atmosphere, causing a contraction of the specimen gauge. Near the end of each half-cycle, the diffusion of hydrogen into or out of the specimen is complete, and the specimen deforms only by steady-state, isochoral creep. The steady-state, isochoral creep predicted by Eq. (1) is shown as dashed lines in Fig. 2, and is in good agreement with the experimental deformation rates measured near the end of the charging or discharging half-cycles. Finally, the strain history during each chemical cycling experiment was identical, within experimental error, for each consecutive chemical cycle at the same stress.

The enhancement in deformation due to chemical cycling is shown in Fig. 3, where the strain increment $\Delta\varepsilon$ developed after each full chemical cycle is plotted as a function of the applied tensile stress σ. The amount of strain expected due to creep (following Eq. (1)) at a constant composition (H-free or H-saturated) is shown for comparison. Whereas isochoral creep strain developed over a fixed duration is expected to follow a power-law relationship with a stress exponent of about 2.8 (Fig. 1), the deformation during chemical cycling is characterized by a stress exponent near unity, and is significantly more rapid than the expected power-law creep in the studied stress range. Finally, we note that the deformation during chemical cycling was approximately equal for the 24- and 30-minute chemical cycles, indicating that the specimens were completely charged with hydrogen within 12 minutes. Since deformation during chemical cycling is fast compared to creep without cycling, the additional 6 minutes of creep (30- compared to 24-minute cycles) do not appreciably increase the average rate of deformation during cycling.

The observed stress exponent of unity (Fig. 3) and the enhanced rate of deformation observed during chemical cycling (Figs. 2,3) are the defining characteristics of internal stress plasticity, and indicate that the internal stresses due to the gradient in lattice swelling are sufficient to activate this deformation mechanism. To our knowledge, this is the first direct observation of internal stress plasticity due solely to swelling mismatch during a process of cyclic alloying/dealloying. Our results are also in agreement with the recent studies of Frary et al. [26] and Zwigl and Dunand [27, 28], who investigated uniaxial deformation during cyclic charging of unalloyed titanium with hydrogen, under conditions where the chemical cycles induced the titanium α/β allotropic transformation. The latter authors found a linear relationship between $\Delta\varepsilon$ and σ, but noted that the internal stress generation was due to a complex superposition of chemical stresses due to lattice swelling and transformation stresses due to the mismatch in density between α- and β-Ti. The present results are in line with these studies, and further demonstrate that swelling mismatch due to a hydrogen concentration gradient can produce sufficient internal stresses to induce internal stress plasticity, without the necessity of a phase transformation.

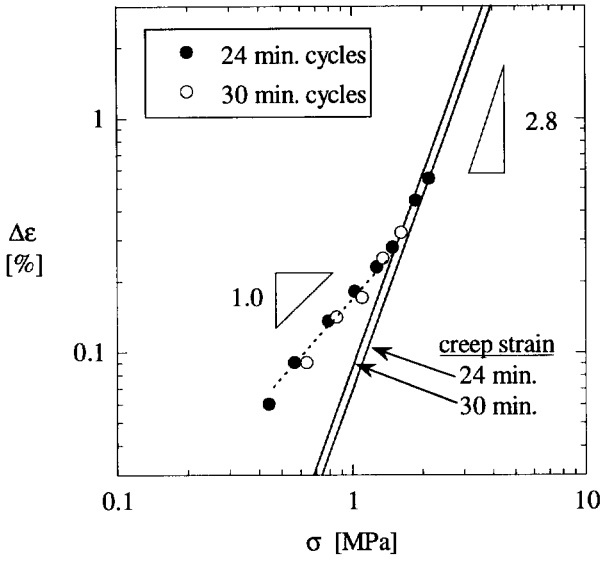

Figure 3: Strain increment $\Delta\varepsilon$ developed after each chemical cycle, plotted as a function of the applied tensile stress σ. The strain expected by creep without chemical cycling is also shown for comparison.

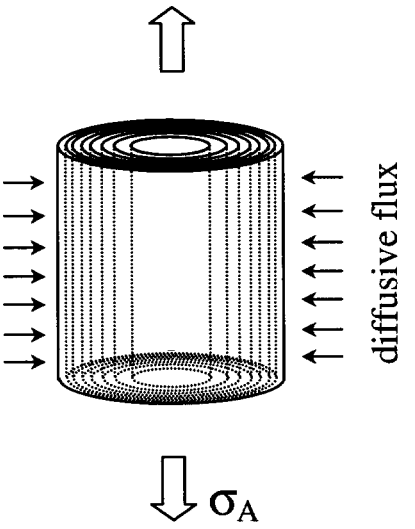

Figure 4: Cylindrical geometry considered in the analytical model, assumed to be very long in the tensile axis, and divided into N concentric elements (N = 8 is shown here).

Modeling Internal Stress Plasticity Due to Chemical Stresses

As described in the Introduction, there are many possible mechanisms for internal stress plasticity, including thermal expansion mismatch, compressibility mismatch, and phase transformation mismatch. Accordingly, there have been many models proposed to predict the stress dependence of the deformation during thermal or pressure cycling [3, 9, 29, 30]. In this section, we describe an analytical model developed in detail in Ref. [31] describing uniaxial deformation under the action of an external stress and internal chemical stresses, which arise due to lattice swelling upon the introduction/removal of a diffusant. The model is based upon the following three main assumptions:

(1) The model considers uniaxial deformation of a very long (infinite) specimen of uniform cross section, under a constant applied stress σ_A in the long dimension. For the purposes of the calculations, the specimen cross-section is divided into N units of infinite length with equal cross-sectional area; for the infinite cylinder considered here (Fig. 4), concentric annular shells are chosen.

(2) The stress state in the specimen is assumed to be purely uniaxial and transverse stresses are neglected. This simplified approach was selected primarily because it does not require that the cross-sectional geometry be specified. The details of the cross-sectional geometry are thus only important as regards the diffusion problem. In the present work we consider the specific case of a long cylinder (circular cross-section), but the uniaxial model allows for ready adaptation to any other cross-sectional geometry.

(3) In the model, chemical stress gradients are produced upon introduction of a diffusant at the surface of the specimen. Because the specimen is very long in one dimension, diffusion is taken to occur only in the plane perpendicular to the stress axis. Additionally, the applied stress is assumed small enough that it does not impact the diffusivity of the diffusant species. In the practical cases to be considered later, the stress range of interest is $\sigma_A < 5$ MPa, for which this assumption is reasonable.

Following the assumption of a purely uniaxial stress state, the N elements in the specimen with stress σ_i and cross-sectional area A_i (i = 1 to N) must obey an axial force balance:

$$\sum_{i=1}^{N} \sigma_i \cdot A_i = \sigma_A \cdot A \tag{2}$$

where A is the total cross-sectional area of the specimen. In addition, strain compatibility requires that strain ε_i be equal in all of the elements:

$$\varepsilon_i = \varepsilon_{i-1}, \qquad (\text{i} = 2 \text{ to N}) \tag{3}$$

We consider situations in which the material sustains plastic deformation by creep, where the creep strain rate, $\dot{\varepsilon}_i^c$, obeys a power-law in stress:

$$\dot{\varepsilon}_i^c = sign(\sigma_i) \cdot K_i \cdot \left|\sigma_i\right|^{n_i} \tag{4}$$

where $\text{sign}(\sigma_i)$ denotes the sign of the stress (positive for tension or negative for compression), K_i is a temperature-dependent constant, and n_i is the power-law stress exponent. At any instant in time, the material can also sustain elastic strains given by Hooke's law, which, if the Young's modulus, E, in each element is independent of time, can be written as:

$$\dot{\varepsilon}_i^e = \frac{\dot{\sigma}_i}{E_i} \tag{5}$$

The instantaneous strain rate in each element is thus composed of these two deformation contributions (elasticity and creep), and a third contribution due to chemical swelling, $\dot{\varepsilon}_i^s$:

$$\dot{\varepsilon}_i = \dot{\varepsilon}_i^c + \dot{\varepsilon}_i^e + \dot{\varepsilon}_i^s \tag{6}$$

where the swelling strain rate in a cylindrical shell of outer and inner radius r^{outer} and r^{inner} is given by [31]:

$$\dot{\varepsilon}_i^s = \frac{c_o - c_s}{\left(r_i^{outer}\right)^2 - \left(r_i^{inner}\right)^2} \cdot \frac{4}{a} \cdot D \cdot F \cdot \sum_{m=1}^{\infty} \exp\left(-D \cdot \alpha_m^2 \cdot t\right) \cdot \frac{r_i^{outer} \cdot J_1\left(r_i^{outer} \cdot \alpha_m\right) - r_i^{inner} \cdot J_1\left(r_i^{inner} \cdot \alpha_m\right)}{J_1\left(a \cdot \alpha_m\right)} \tag{7}$$

with D the diffusivity of the diffusant species, F a swelling proportionality constant (see, e.g., Refs. [26, 31] for a review of the physics of chemical volume changes), J_x the Bessel function of the first kind of order x, and α the positive roots of J_0. Equation (7) is based on the solution to Fick's second law of diffusion, assuming square chemical waves, with a surface concentration of c_s and an initial uniform concentration c_o. As described in detail in Ref. [31], when all of the elements are chosen to have equal cross-sectional areas, the above system of equations can be solved for a given choice of N in closed form, giving a recursive relationship for the rates of stress change, $\dot{\sigma}_i$, where the first term (at the cylinder surface) is given by:

$$\dot{\sigma}_1 = \frac{E}{N} \cdot \sum_{j=2}^{N} b_j \cdot (N + 1 - j) \tag{8a}$$

and each subsequent term is computed by iterating the value of i and using:

$$\dot{\sigma}_i = \dot{\sigma}_{i-1} - E \cdot b_i \qquad (\text{i} = 2 \text{ to N}) \tag{8c}$$

where:

$$b_i = \dot{\varepsilon}_i^s - \dot{\varepsilon}_{i-1}^s + sign(\sigma_i) \cdot K_i \cdot \left|\sigma_i\right|^{n_i} - sign(\sigma_{i-1}) \cdot K_{i-1} \cdot \left|\sigma_{i-1}\right|^{n_{i-1}} \qquad (\text{i} = 2 \text{ to N}) \tag{9}$$

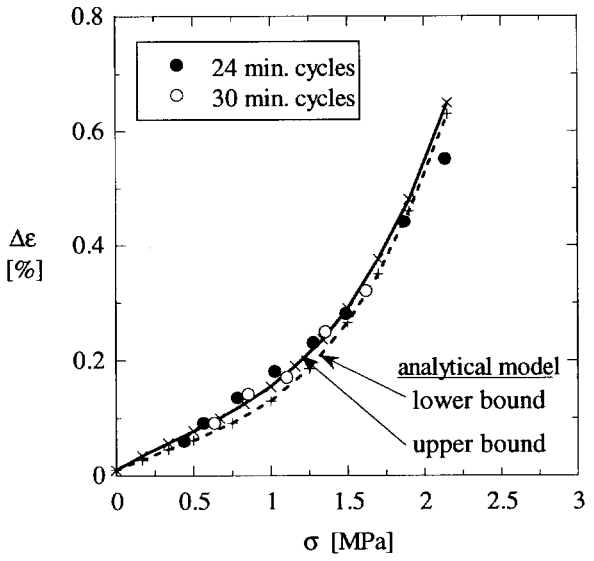

Figure 5: Strain increment after each complete chemical cycle as a function of the applied tensile stress (from Fig. 3), compared with the predictions of the analytical model.

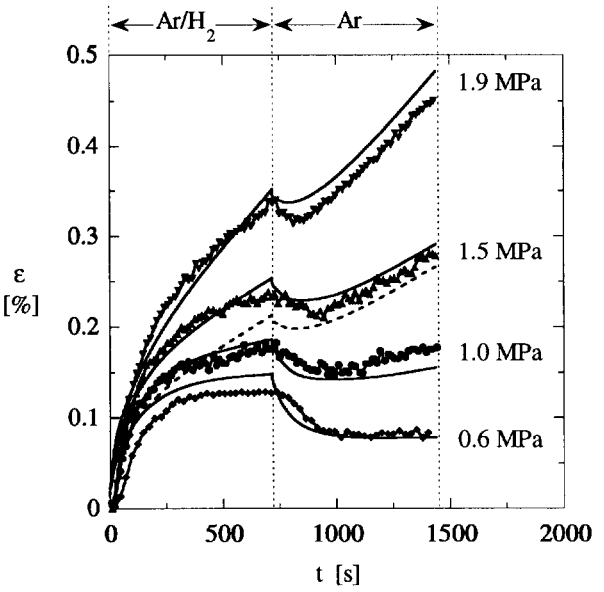

Figure 6: Strain evolution during a single 24-minute chemical cycle, experimental data (points) compared with the model predictions (lines), using the upper-bound swelling constant (solid lines), or the lower-bound value (dashed line).

Simulation of the dynamic process of chemical cycling involves computing the stress state at many discrete moments during the cycle. At any instant in time, the stress state is fully known, and the rate of change of that stress state is calculated from Eq. (8). Then, a finite time step Δt is applied and the stress in each element, as well as the strain of the specimen, are updated using a forward-difference approximation; in this formulation, the constant applied stress is introduced as an initial condition; at $t = 0$, $\sigma_i = \sigma_A$, for $i = 1$ to N. Further details of the derivation and computational procedures are available in Ref. [31].

Comparison with Experiment

In applying this model to the present experiments, we employ a cylindrical geometry with a radius of a = 2.5 mm. During the experiments, this radius decreased somewhat (at most by ~9%) due to plastic elongation of the specimens, but this contraction was found to produce no significant variation in the predictions of the model. In the calculations, N = 100 concentric annuli of equal cross-sectional area are chosen, and the stress and strain state in each is tracked during a 24-minute chemical cycle. The first half of the cycle involves diffusion with a fixed hydrogen concentration $c_s = c_{eq}$ at the surface, and the second half-cycle involves a fixed surface concentration of $c = 0$; the specimen is either hydrogen-free or -saturated at the beginning of each half-cycle. A narrow range of physically-reasonable swelling proportionality constants has been determined from the present experimental data in Ref. [31] as $F = 0.0008/c_{eq} - 0.0011/c_{eq}$; both of these values are used in the model to establish upper and lower bound predictions. The shear modulus of β-Ti at 1030° C is G = 16 GPa [32], from which the Young's modulus E = 44 GPa is calculated using $E = 2 \cdot G \cdot (1+\nu)$, where the Poisson's ratio of β-Ti is taken as $\nu = 0.36$ [33]. The creep behavior of Ti-6Al-4V at 1030° C is described by Eq. (1), using the parameters determined experimentally ($K = 4.8 \cdot 10^{-7}$ $MPa^{-2.8}s^{-1}$ and n = 2.8, Fig. 1). Finally, the diffusivity of atomic hydrogen in various β-Ti alloys (but not Ti-6Al-4V) spans

a broad range ($5 \cdot 10^{-6}$-$3 \cdot 10^{-4}$ cm^2/s) at 1030° C [34]; we take here an average value, $D = 7.5 \cdot 10^{-5}$ cm^2/s.

This model, with the input parameters described above, requires no additional adjustable parameters, and its predictions can be directly compared with the experimental data. Of particular interest is the strain increment accumulated after a complete chemical cycle, $\Delta\varepsilon$. In Fig. 5, the experimental values of $\Delta\varepsilon$ from Fig. 3 are plotted against the applied stress, on linear axes. At low stresses, the data points fall on a line, with a deviation to a larger stress-dependence as the stress is increased. Shown for comparison are the predictions of the analytical model (using both the upper- and lower-bound values for the swelling proportionality constant, F) demonstrating good qualitative and quantitative agreement with the data. Additionally, the model predictions are successful over the full range of investigated stresses, both at low stresses, where the model and data exhibit the linear $\Delta\varepsilon$ vs. σ relationship expected for internal-stress plasticity, and at higher stresses, where the data and model both exhibit a smooth divergence to larger strain increments. This divergence is also typical for internal-stress plasticity by thermal cycling [8, 13, 29, 35]; when the external stress is very large compared to the internal stresses, deformation occurs primarily due to the external stress, according to the typical deformation power-law of the material.

In addition to the net deformation after a complete chemical cycle, the model is also capable of predicting the complete strain history during a hydrogen cycle. In Fig. 6, the predicted evolution of strain is shown for four different applied stresses, and compared with experimental data. The model predicts the shape of the curves with accuracy, including the rate of swelling expansion/contraction, the steady-state deformation observed after the completion of charging or discharging, and the total strain developed at the end of the cycle (Fig. 6).

In Figs. 5 and 6, the small disagreement between the model and the experiments can be traced to several factors, including uncertainty in the hydrogen diffusivity and creep parameters, the assumption of instantaneous hydrogen sorption and desorption at the specimen surface, and the simplified uniaxial stress state. However, the model predicts the average strain rate during thermal cycling to within about 15% over the stresses investigated. We thus believe that a more complex modeling approach would only achieve marginal improvements in predictive power, and this simplified approach captures the essential physics and mechanics of deformation under chemical cycling conditions.

Conclusions

Internal stress plasticit$^{\text{lower bound}}$ the simultaneous presence of internal mismatch stresses and an external stress.$^{\text{upper bound}}$ biasing the former. In the present work, we have experimentally demonstrated that internal stress plasticity can occur due to the presence of chemical stresses, caused by dynamic concentration gradients produced by cyclic charging/discharging of β-phase Ti-6Al-4V with hydrogen. Tensile deformation experiments at 1030° C involved alternating exposure to pure argon and an argon/hydrogen mixture. The cyclic absorption and desorption of hydrogen in solid solution within the metal induced chemical stresses, which were biased by the external tensile stress. The main points of this work are listed below:

- In a static atmosphere of either pure Ar or Ar/3.66% H_2, β-phase Ti-6Al-4V deforms by power-law creep with a stress exponent near three at low stresses (below about 5 MPa). Dissolved hydrogen does not significantly impact the isothermal creep behavior of the alloy.

- During chemical cycles of 24 or 30 minutes duration, specimens were found to deform at rates faster than by isochoral creep in a constant atmosphere, particularly at stresses below about 1.5 MPa. Additionally, the average strain rate during chemical cycling was found to be

proportional to the applied stress. These two characteristics demonstrate the operation of internal stress plasticity during chemical cycling.

• A new analytical model has been developed to consider the effect of diffusion and chemical strains on uniaxial creep. The model has been applied to our experimental data using input parameters determined experimentally in this work and taken from the literature, but without adjustable parameters. It predicts the strain evolution during chemical cycling with accuracy, as well as the strain developed after a complete cycle within about 15% for all of the investigated stresses.

Acknowledgements- This study was funded by the National Science Foundation, under grant DMR-9987593. C.S. also acknowledges the U.S. Department of Defense for a National Defense Science and Engineering Graduate Fellowship, as well as the University of California Lawrence Livermore National Laboratory (under the U.S. Department of Energy Contract W-7405-Eng-48) for a Lawrence Livermore Postdoctoral Fellowship.

References

1. T.G. Nieh, J. Wadsworth, and O.D. Sherby, Superplasticity in Metals and Ceramics (Cambridge: Cambridge University Press, 1997).
2. S.M. Pickard and B. Derby, "The Deformation of Particle Reinforced Metal Matrix Composites During Temperature Cycling." Acta Metall. Mater., 38 (1990). 2537-52.
3. G.S. Daehn and T. Oyama, "The Mechanism of Thermal Cycling Enhanced Deformation in Whisker-Reinforced Composites." Scripta Metall. Mater., 22 (1988). 1097-102.
4. K. Kitazono and E. Sato, "Internal Stress Superplasticity in Al-Be Eutectic Alloy During Triangular Temperature Profile." Acta Mater., 46 (1998). 207-13.
5. K. Kitazono and E. Sato, "Internal Stress Superplasticity in Directionally Solidified Al-Al_3Ni Eutectic Composite." Acta Mater., 47 (1999). 135-42.
6. S.M. Pickard and B. Derby, "The Influence of Microstructure on Internal Stress Superplasticity in Polycrystalline Zinc." Scripta Metall. Mater., 25 (1991). 467-72.
7. K. Kitazono, et al., "Effects of Crystallographic Texture on Internal Stress Superplasticity Induced by Anisotropic Thermal Expansion," in Superplasticity : Current Status and Future Potential, P.B. Berbon, et al.: MRS, Warrendale PA, 2000), 199-204.
8. M.Y. Wu, J. Wadsworth, and O.D. Sherby, "Internal Stress Superplasticity in Anisotropic Polycrystalline Zinc and Uranium." Metall. Trans., 18A (1987). 451-62.
9. G.W. Greenwood and R.H. Johnson, "The Deformation of Metals Under Small Stresses during Phase Transformations." Proc. Roy. Soc. Lond., 283A (1965). 403-22.
10. F.W. Clinard and O.D. Sherby, "Strength of Iron during Allotropic Transformation." Acta Metall., 12 (1964). 911-9.
11. R. Kot, G. Krause, and V. Weiss, "Transformation Plasticity of Titanium," in The Science, Technology and Applications of Titanium, R.I. Jaffe and N.E. Promisel (Oxford: Pergamon, 1970), 597-605.
12. C. Schuh and D.C. Dunand, "Transformation Superplasticity of Super Alpha-2 Titanium Aluminide." Acta Mater., 46 (1998). 5663-75.
13. C. Schuh and D.C. Dunand, "Non-Isothermal Transformation-Mismatch Plasticity: Modeling and Experiments on Ti-6Al-4V." Acta Mater., 49 (2001). 199-210.
14. D.C. Dunand and C.M. Bedell, "Transformation-Mismatch Superplasticity in Reinforced and Unreinforced Titanium." Acta Mater., 44 (1996). 1063-76.
15. P. Zwigl and D.C. Dunand, "Transformation Superplasticity of Zirconium." Metall. Mater. Trans., 29A (1998). 2571-81.
16. D.C. Dunand and J.G. Grabowski, "Tensile Transformation Plasticity of Bismuth Oxide." J. Am. Ceram. Soc., 83 (2000). 2521-8.

17. C.Y. Huang and G.S. Daehn, "Superplastic Forming of Metal Matrix Composites by Thermal and Pressure Cycling," in Superplasticity and Superplastic Forming 1995, A.K. Ghosh and T.R. Bieler, eds. (Warrendale, PA: TMS, 1996), 135-42.
18. C.-Y. Huang and G.S. Daehn, "Effect of Cyclic Pressure on the Low Temperature Consolidation of Several Composite Powder Systems." Acta Mater., 45 (1997). 4283-96.
19. D.C. Dunand, C. Schuh, and D.L. Goldsby, "Pressure-Induced Transformation Plasticity in H_2O Ice." Phys. Rev. Lett., 86 (2001). 668-71.
20. J.C.-M. Li, "Physical Chemistry of Some Microstructural Phenomena." Metall. Trans., 9A (1978). 1353-80.
21. W. Szkliniarz and G. Smolka, "Analysis of Volume Effects of Phase Transformation in Titanium Alloys." J. Mater. Proc. Tech., 53 (1995). 413-22.
22. D. Eliezer, et al., "Positive Effects of Hydrogen in Metals." Mater. Sci. Eng., A280 (2000). 220-4.
23. O.N. Senkov and J.J. Jonas, "Effect of Phase Composition and Hydrogen Level on the Deformation Behavior of Titanium-Hydrogen Alloys." Metall. Mater. Trans., 27A (1996). 1869-76.
24. T. Seshacharyulu, et al., "Hot Deformation and Microstructural Damage Mechanisms in Extra-Low Interstitial (ELI) Grade Ti-6Al-4V." Mater. Sci. Eng., A279 (2000). 289-99.
25. T. Seshacharyulu, et al., "Hot Deformation Mechanisms in ELI Grade Ti-6Al-4V." Scripta Mater., 41 (1999). 283-8.
26. M. Frary, C. Schuh, and D.C. Dunand, "Strain Ratchetting of Titanium Upon Reversible Alloying with Hydrogen." Phil. Mag. A, 81 (2001). 197-212.
27. D.C. Dunand and P. Zwigl, "Hydrogen-Induced Internal-Stress Plasticity in Titanium." Metall. Mater. Trans., 32A (2001). 841-3.
28. P. Zwigl and D.C. Dunand, "Transformation Superplasticity by Cyclic Alloying with Hydrogen." J. Mater. Proc. Tech., (in print).
29. E. Sato and K. Kuribayashi, "A Model of Internal Stress Superplasticity Based on Continuum Mechanics." Acta Metall. Mater., 41 (1993). 1759-67.
30. B. Derby, "Internal Stress Superplasticity in Metal Matrix Composites." Scripta Metall., 19 (1985). 703-7.
31. C. Schuh and D. C. Dunand, "Internal Stress Plasticity due to Chemical Stress Gradients." Acta Mater., in print (2001).
32. H.J. Frost and M.F. Ashby, Deformation-Mechanism Maps: The Plasticity and Creep of Metals and Ceramics, (Oxford: Pergamon Press, 1982).
33. O.N. Senkov, M. DuBois, and J.J. Jonas, "Elastic Moduli of Titanium-Hydrogen Alloys in the Temperature Range 20 C to 1100 C." Metall. Mater. Trans., 27A (1996). 3963-70.
34. H.-J. Christ, M. Decker, and S. Zeitler, "Hydrogen Diffusion Coefficients in the Titanium Alloys IMI 834, Ti 10-2-3, Ti 21 S, and Alloy C." Metall. Mater. Trans., 31A (2000). 1507-17.
35. P. Zwigl and D.C. Dunand, "A Non-Linear Model for Internal Stress Superplasticity." Acta Mater., 45 (1997). 5285-94.